Remote Sensing-Based Estimation of Mangrove Above-Ground Carbon Using Sentinel-2 Vegetation Indices and Random Forest

Aulia Lanudia Fathah
Master Program of Environmental Management & Development, Brawijaya University, Indonesia
aulialf@student.ub.ac.id

Bambang Semedi
Master Program of Environmental Management & Development, Brawijaya University, Indonesia
bambangsemedi@ub.ac.id

Fitri Candra Wardana
Master Program of Environmental Management & Development, Brawijaya University, Indonesia
fitri_fia@ub.ac.id

Andik Isdianto
Department of Marine Science, Brawijaya University, Indonesia
andik.isdianto@ub.ac.id (corresponding author)

Received: 26 August 2025 | Revised: 10 September 2025, 23 September 2025, and 28 September 2025 | Accepted: 6 October 2025

 DOI: https://doi.org/10.48084/etasr.14335

ABSTRACT

Mangrove ecosystems are critical blue carbon reservoirs. Accurate estimation of Above-Ground Carbon (AGC) is essential for climate change mitigation and coastal management. This study applies Sentinel-2 multispectral imagery and vegetation indices with a Random Forest model to estimate mangrove AGC in fragmented coastal ecosystems of Ujungpangkah, Indonesia. Field-based AGC from 15 plots, derived using species-specific allometry, was integrated with Google Earth Engine processing of spectral bands and indices. The classification mask achieved high accuracy (OA = 0.946; κ = 0.810). Among predictors, the Shortwave Infrared Bands (SWIR; B11–B12) and the Transformed Vegetation Index (TRVI) were the most effective, outperforming traditional red-edge indices. External validation showed reliable performance (R^2 = 0.65; RMSE ≈ 1.05 tons C/ha), while the mapped mangroves averaged 25.3 tons C/ha, totaling ~2,036.5 tons C. SWIR was negatively correlated with AGC due to canopy water and structure, whereas TRVI captured canopy variability and reduced saturation. These findings highlight the potential of integrating Sentinel-2 imagery and vegetation indices with machine learning to provide cost-effective and replicable blue carbon monitoring for mangrove management.

Keywords-blue carbon; Google Earth Engine; SWIR; TRVI; random forest modeling; coastal carbon mapping; tropical mangrove monitoring

I. INTRODUCTION

Global warming is driven by increasing anthropogenic greenhouse gas emissions [1]. Mangroves play a crucial role in the mitigation of climate change by significantly contributing to the global carbon cycle and reducing atmospheric CO_2 levels [2]. They also offer economic potential through blue-carbon initiatives in Indonesia [3], holding the largest blue-carbon pool, estimated at 6.5 billion tons [4]. Reliable methods are therefore essential to monitor mangrove carbon sequestration and improve carbon stock estimation, highlighting the need for accurate and replicable assessment approaches.

Remote sensing based on multispectral imagery and vegetation indices has emerged as one of the most effective approaches to estimating mangrove Above-Ground Carbon (AGC). This method provides a broad spatial coverage and time efficiency [5]; however, its application in small or fragmented mangrove areas requires careful synchronization with field data [6]. Such conditions often require specific model adjustments to accurately capture structural variability and vegetation composition [7]. Vegetation indices such as NDVI, EVI, and TRVI have been widely used for vegetation monitoring. In similar remote-sensing applications, it has been

shown that combining NDWI with AI and GIS can enhance environmental change detection using multitemporal imagery [8], underscoring the importance of integrating spectral indices with advanced modeling approaches.

Previous studies have utilized multispectral satellite imagery and vegetation indices to estimate mangrove AGC, demonstrating the potential of remote sensing for large-scale assessments [3, 7]. However, many of these approaches rely on generalized models with limited ground-truth calibration, which can reduce accuracy in small, fragmented, or degraded mangrove systems. In addition, the spatial heterogeneity and land-use pressures in such ecosystems call for site-specific modeling and validation, which remain underexplored in the literature.

This study uses Sentinel-2 imagery to map mangrove AGC in the Banyuurip Mangrove Center (BMC) and Lewean Mangrove Park (LMP) site with pronounced conversion and sedimentation pressures [9]. A vegetation-index-based Random Forest (RF) model was calibrated with plot-level AGC to explore the predictive performance of different spectral features. The contributions of this study are twofold: (i) shows that SWIR bands (B11–B12) and TRVI consistently outrank red-edge indices for AGC prediction (R^2, RMSE, and feature-importance ranks), and (ii) provides a field-validated 10–20 m AGC map suitable for blue-carbon MRV, with strong cross-validated performance (OA/Kappa for AGC classes, R^2 and RMSE for regression). Unlike studies highlighting NIR/red-edge or IRECI dominance, the results show that SWIR and TRVI are superior in these site conditions, pointing to context-dependent feature importance.

II. MATERIALS AND METHODS

A. Study Site

The Banyuurip Mangrove Center (BMC) and Lewean Mangrove Park (LMP), located in the Ujungpangkah District in the Bengawan Solo River Delta, are part of the North Java coastal mangrove system (Figure 1). Covering 1,554 hectares, it is the largest mangrove area in Gresik and among the largest in East Java [10]. However, land conversion has significantly reduced natural mangrove cover, affecting ecological functions and carbon sequestration [11, 12].

B. Data Collection

Figure 2 shows a schematic of the Sentinel-2 data utilization method to build the estimation model of AGC stock in mangroves.

1) Primary Data

Field data were collected from April 25 to 30, 2025, at five observation stations—three in BMC and two in LMP—each consisting of three 10×10 m plots, totaling 15 plots. A non-destructive sampling approach [13] was applied in every plot to collect the following data: (1) identification of the species based on morphological characteristics (leaf, stem, and root); (2) measurement of DBH at 1.3 meters; and (3) measurement of tree height. Of the 15 plots, 11 (75%) were used to develop the model, while 4 (25%) were reserved for independent validation.

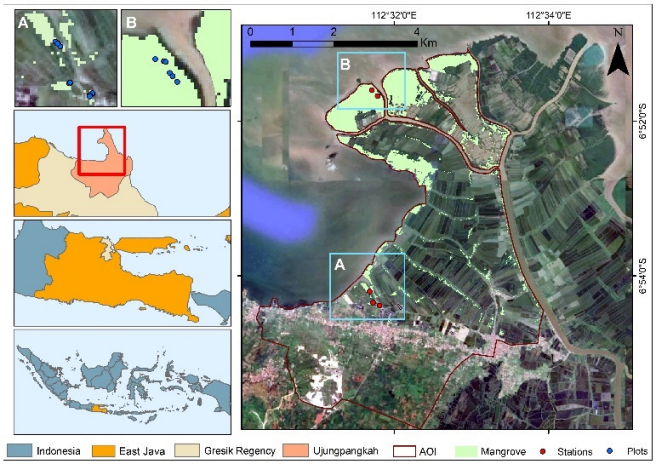

Fig. 1. Study site location in the Ujungpangkah district, Gresik regency.

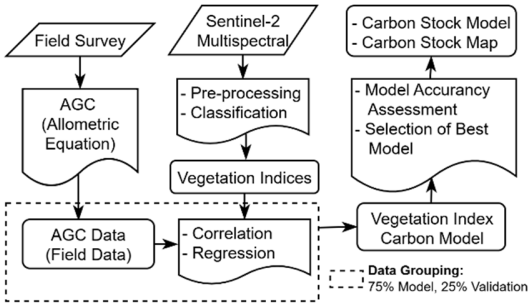

Fig. 2. Flowchart for mapping and calculating the AGC.

2) Secondary Data

Sentinel-2 Level-2A imagery with atmospherically corrected Surface Reflectance (SR) and less than 20% cloud cover was acquired from the COPERNICUS/ S2_SR_HARMONIZED collection in Google Earth Engine (GEE) from January 1 to June 26, 2025, based on a predefined Area of Interest (AoI).

C. Data Processing

1) Image Processing

As shown in Figure 3, image processing comprised three stages. An RF classifier was used for mangrove vs non-mangrove classification, with input features from NIR, SWIR, and Red bands [3, 7]. Vegetation indices (NDVI, EVI, TRVI, and IRECI) were then computed and used as predictors for AGC modeling. All procedures were implemented in GEE and spatially validated using field-sampled plots. Final map products were visualized in ArcGIS 10.8. The RF in Google Earth Engine used 100 trees, with default settings of variables at each split and no depth limit, which are widely applied in ecological remote sensing to balance accuracy and efficiency.

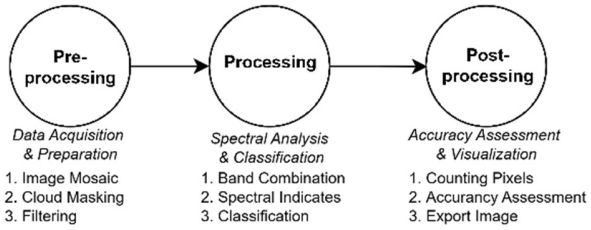

Fig. 3. Flowchart of image processing.

2) Estimation of Above-Ground Carbon (AGC)

Biomass calculations included trees with DBH ≥ 5 cm and height ≥ 1 m [14, 15]. Plot-level Above-Ground Biomass (AGB) was derived from species-specific allometric equations, incorporating species-adjusted wood density ρ [16-18]. AGB was estimated and converted to AGC, as shown in Figure 4, using the formulas below:

$$AGB = 0.251\,\rho\,DBH^{2.46} \quad (1)$$

$$AGC = AGB \times 0.47 \quad (2)$$

Carbon is reported in tons (metric tons). Pixel-to-hectare conversion uses an effective pixel area of 0.04 ha (SWIR-20 m).

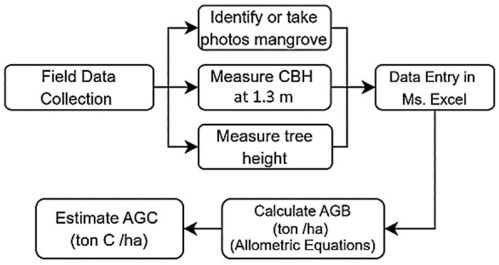

Fig. 4. Flowchart of field data collected for AGC analysis.

3) Accuracy Assessment and Model Validation

The model with the best performance—indicated by the lowest Root Mean Square Error (RMSE) and the highest correlation coefficient (R^2)—was used to estimate and map AGC values across the entire study area [19]. A lower RMSE value indicates higher prediction accuracy [20]. Meanwhile, R^2 was used to evaluate the linear relationship between the observed field AGB values and the model's predictions [21]. The formulas used are as follows:

$$RMSE = \sqrt{\frac{1}{n}\sum_{i=1}^{n}(y_i - \hat{y}_i)^2} \quad (3)$$

$$R^2 = 1 - \frac{\sum_{i=1}^{n}(y_i - \hat{y}_i)^2}{\sum_{i=1}^{n}(y_i - \bar{y})^2} \quad (4)$$

RMSE is reported in tons C/pixel and converted to tons C/ha using 0.04 ha per pixel (SWIR-20 m). For validation, 4 of the 15 plots (25%) were withheld as an independent hold-out set, while 11 plots were used for training. K-fold cross-validation was not applied due to the limited number and clustered distribution of plots, which could bias results. The hold-out approach provides a conservative and realistic estimate of model performance in data-limited mangrove sites.

III. RESULTS AND DISCUSSION

A. Above-Ground Carbon (AGC) Stocks

Table I shows the calculation of AGC at the sample points. Based on these results, plot 4 has the highest AGC value (79.2 tons C/ha) among other sampling plots, while plot 9 has the lowest AGC value (7.1 tons C/ha). The AGC estimation model was built assuming that AGB is closely related to tree diameter (DBH) and wood density. AGB affects the amount of AGC stored in each tree, so an increase in biomass is positively correlated with an increase in carbon [22].

TABLE I. BIOMASS AND CARBON STOCK CALCULATION RESULTS

Sample plots	AGB (ton/ha)	AGC (tons C/ha)	Dominant species
1	126.4	59.4	*Avicennia marina*
2	128.3	60.3	*Avicennia marina*
3	99.5	46.8	*Avicennia marina*
4	168.4	79.2	*Avicennia marina*
5	109.2	51.3	*Avicennia marina*
6	61.7	29.0	*Avicennia marina*
7	33.1	15.6	*Avicennia marina*
8	16.0	7.5	*Avicennia marina*
9	15.1	7.1	*Avicennia marina*
10	64.0	30.1	*Avicennia marina*
11	46.2	21.7	*Rhizopora stylosa*
12	43.4	20.4	*Avicennia marina*
13	54.2	25.5	*Avicennia alba*
14	47.5	22.3	*Rhizopora apiculata*
15	34.7	16.3	*Rhizopora stylosa*

Avicennia marina was found dominant in 11 of 15 plots, including those with the highest (Plot 4) and lowest (Plot 9) AGC. Other dominants were *Rhizophora stylosa* (Plot 11 and 15), *Avicennia alba* (Plot 13), and *Rhizophora apiculata* (Plot 14). *Avicennia marina* exhibited widespread dominance, while *Rhizophora* species and *Avicennia alba* were locally dominant. This variation in species dominance correlates with AGC differences, highlighting the role of species composition.

B. Image Classification and Extraction of Mangrove Forests

The detected mangrove area during the period of January – July 2025 in the study site was approximately 286.19 ha (Figure 5). The classification of mangrove and non-mangrove areas using RF based on several parameters resulted in relatively high accuracy, with an Overall Accuracy (OA) of 0.946 and a Kappa (κ) coefficient of 0.810. These results indicate strong agreement with field observations, as reflected by the high Kappa coefficient [19].

C. Relationship of Field AGC and Spectral Reflectance

The correlation analysis revealed a relatively strong negative relationship for SWIR reflectance, particularly for B11 ($r = -0.749$) and B12 ($r = -0.609$) (Figure 6). This observation indicates that increased reflectance in SWIR reflectance corresponds to lower AGC in mangrove canopies. However, the pattern is not uniform across plots: subset correlations reveal heterogeneity, with Plots 1-4 showing weak/inconsistent relationships (B11 $r = +0.1$, B12 $r = -0.05$), whereas Plots 5–14 exhibit stronger negative associations (B11 $r = -0.48$, B12 $r = -0.84$), consistent with the non-uniform pattern in Figure 6.

Among the tested indices, TRVI showed the strongest positive correlation with AGC ($r = 0.389$), indicating its higher sensitivity to mangrove biomass. In contrast, NDVI, EVI, and IRECI exhibited weak and negative correlations, suggesting their limited effectiveness in capturing carbon variability in dense mangrove canopies (Figure 7). These results suggest that SWIR bands and TRVI provide the most informative predictors for modeling AGC in the study area.

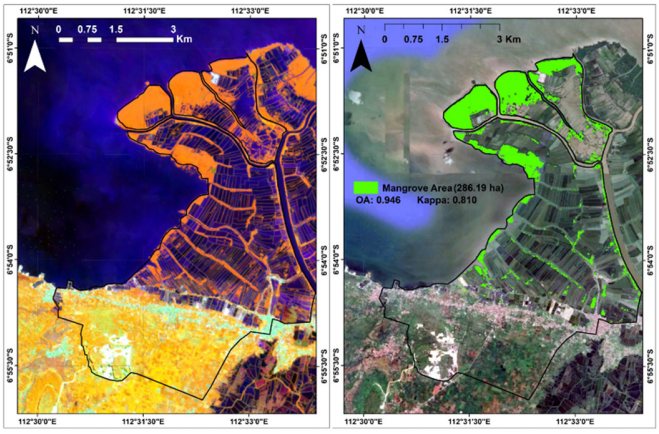

Fig. 5. False color composite (NIR, SWIR, Red) (left) and RF-based mangrove classification (right).

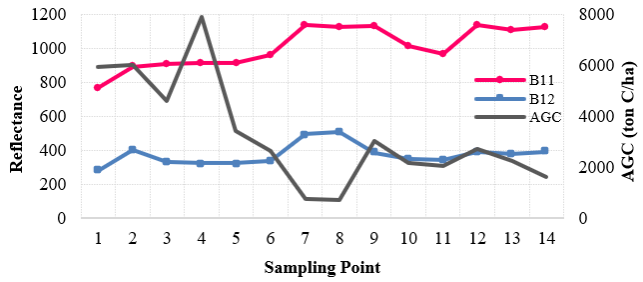

Fig. 6. Relationship of mangrove band indices and field-measured AGC.

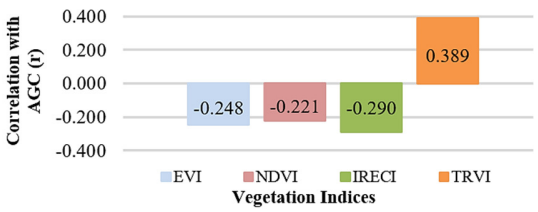

Fig. 7. Relationship of vegetation indices and field-measured AGC.

D. Mangrove Carbon Predictive Mapping

The Sentinel-2/RF model produced an operational per-pixel AGC surface for the Ujungpangkah mangroves (Figure 8). Internal accuracy in GEE was high ($R^2 = 0.787$; RMSE = 0.042 tons C pixel^{-1} ≈ 1.05 tons C ha^{-1} at 20 m; MAE = 0.041 tons C pixel^{-1} ≈ 1.03 tons C ha^{-1}). External validation against field-measured AGC (Figure 1) showed a moderate–strong fit ($R^2 = 0.65$; $\hat{y} = 0.3288\,x + 0.8805$). The slope of less than one with a positive intercept indicates a mild compression of the prediction range (slight overestimation at low AGC and underestimation at high AGC).

The mapped surface displays a coherent spatial gradient (Figure 8). Higher AGC values cluster within more continuous mangrove blocks, whereas lower values occur along fragmented fringes and aquaculture margins. Over the mapped mask, the predicted mean AGC is 25.3 tons C ha^{-1}, yielding an estimated total stock of approximately 2,036.5 tons C. Pixel values shown in the legend span 0.22–0.46 tons C pixel^{-1} (~5.5–11.5 tons C ha^{-1} using a 0.04-ha pixel).

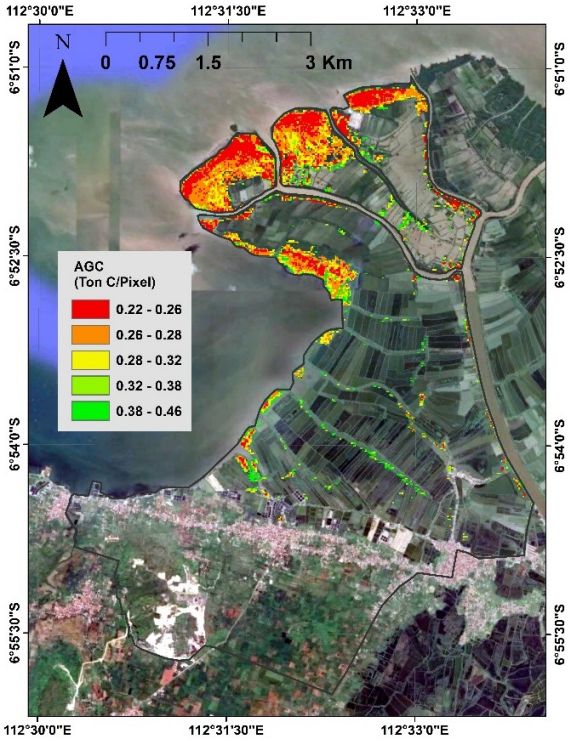

Fig. 8. Estimated mangrove AGC in Ujungpangkah (tons C/pixel, pixel = 20 m). Conversion to tons C/ha uses factor 25 (1 pixel = 0.04 ha)

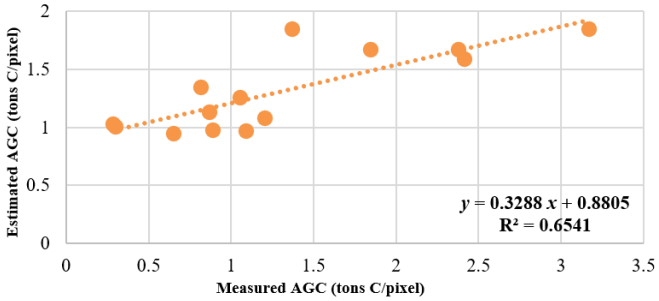

Fig. 9. Validation of the RF AGC model using field plots. Relationship between measured and predicted AGC (tons C/pixel); $\hat{y}$ = 0.3288 x + 0.8805; R^2 = 0.65.

E. Discussion

The mapped AGC surface delineates an ecologically plausible mosaic in Ujungpangkah: higher values cluster in more continuous stands and along well-flushed tidal creeks/headlands, while lower values occur on fragmented fringes near aquaculture margins. Over the mapped mask, the surface yields a mean of 25.3 tons C/ha and ~2,036.5 tons C in

total, consistent with the pixel legend when converting from tons C pixel^{-1} to tons C ha^{-1} for 20 m pixels. These patterns align with small-area remote-sensing applications that report coherent, management-relevant blue carbon gradients.

The external/hold-out validation highlights the abilities of the model, with $R^2 = 0.65$, regression $\hat{y} = 0.3288\,x + 0.8805$, and RMSE = 0.042 tons C/pixel (~1.05 tons C/ha). The robust mangrove/non-mangrove mask (OA = 0.946; κ = 0.810) helps limit error carry-over from classification to regression. Internal fit (OOB) is higher ($R^2 \approx 0.787$), but the hold-out metric is treated as a conservative, generalizable estimate. Comparable studies stress a clear separation between internal and external validation to avoid optimism bias [23, 24].

Spectrally, SWIR reflectance (B11–B12) is negatively associated with AGC ($r = -0.749$; -0.609), consistent with its sensitivity to canopy/leaf water content and structural density in tidal forests. Among the tested indices, TRVI shows the strongest positive correlation with AGC ($R^2 = 0.389$), whereas NDVI, EVI, and IRECI exhibit weak negative associations (Figures 6 and 7). Table II presents a summary of these patterns from the literature.

TABLE II. R^2 AND RMSE (TONS C/HA) FOR SENTINEL-2 BANDS AND VEGETATION INDICES IN MANGROVE AGC PREDICTION

Predictor/s	R^2		RMSE (±tons/ha)	
	[7]	[3]	[7]	[3]
Multispectral bands				
Red Edge 1	0.06	0.10	25.17	25.34
Red Edge 2	0.59	0.80	24.30	18.31
Red Edge 3	0.60	0.81	23.21	16.51
NIR	0.66	0.86	30.50	20.04
SWIR	0.36	0.19	18.30	26.04
Vegetation indices				
NDVI	0.73	0.82	26.06	18.65
TRVI	0.76	0.88	26.00	18.57
IRECI	0.76	0.89	17.14	13.72

Benchmarking against prior studies, TRVI consistently performs well, with $R^2 \approx 0.76$ and RMSE ≈ 26.00 tons C/ha [7] and $R^2 \approx 0.88$ and RMSE ≈ 18.57 tons C/ha [3]. Notably, these studies also report NIR, Red-Edge 2, and Red-Edge 3 among stronger predictors, highlighting their typical dominance in Table II. In contrast, single-band SWIR shows mixed performance across sites, with $R^2 \approx 0.36$ and RMSE ≈ 18.30 tons C/ha in [7] versus $R^2 \approx 0.19$ and RMSE ≈ 26.04 tons C/ha in [3]. In the sites used in this study, SWIR (negative) and TRVI (positive) emerge as the top predictors and yield the best cross-validated performance, suggesting that canopy-water and structural controls under conversion/sedimentation pressures drive a context-dependent dominance of SWIR and TRVI.

The context-specific dominance of SWIR and TRVI in Ujungpangkah is strongly influenced by local environmental conditions. The deltaic setting with muddy substrates and pronounced tidal flushing makes the canopy water content a critical driver of the spectral response, explaining the strong negative association between SWIR and AGC, since SWIR is sensitive to canopy/leaf water content levels, a crucial factor in mangrove habitats influenced by tidal dynamics [25]. In addition, land conversion to aquaculture and salinity stress create structural heterogeneity in mangrove stands, particularly within the *Avicennia marina*, the dominant species on 11 of 15 plots. Under these conditions, conventional indices, such as NDVI and EVI, tend to saturate in dense canopies, while TRVI reduces saturation effects and better reflects canopy structure, enabling it to capture variability in fragmented patches more effectively. These ecological and structural factors jointly explain why SWIR and TRVI outperform red-edge indices in this study area.

The field composition corroborates the mapped gradients: *Avicennia marina* dominates 11/15 plots and spans local extremes (Plot 4: 79.2 tons C/ha; Plot 9: 7.1 tons C/ha), indicating that species mix, stand continuity/age, and edge exposure jointly shape the AGC mosaic. *Avicennia marina* shows the highest contributions as a fast-growing pioneer with widespread coverage, whereas *Rhizophora* species, with higher wood density (ρ), salinity tolerance, and stilt roots adapted to higher wave energy, contribute to long-term carbon storage [26-28]. Similar links between dominant taxa, structure, and carbon distribution are reported in small-site studies [3, 7]. The mean AGC of 32.7 tons C/ha observed in BMC and LMP is lower than values reported for nearby island mangroves such as Bawean (~50.98 tons C/ha), although the latter includes both above- and below-ground components [10].

A priority for protecting high-AGC involves preventing conversion and illegal logging through clear enforcement and community co-management. For low-AGC zones (e.g., abandoned ponds and fragmented fringes), the hydrology must be restored, followed by replanting. Community-based ecotourism can reinforce compliance and sustain gains. On a national scale, conservation plus restoration provides meaningful mitigation [29, 30].

However, this study has limitations, as the number of plots examined and their spacing limit the dynamic range and spatial independence. In addition, mixed-pixel effects are plausible at 20 m, and texture/ancillary biophysical variables were not included. Future studies should expand plot coverage and spacing, evaluating red-edge–SWIR pairings and multi-temporal imagery. However, the proposed workflow still provides a practical baseline for local management and blue-carbon MRV.

IV. CONCLUSION

This study presented an integrated workflow for estimating mangrove AGC by combining field data from 15 plots with Sentinel-2 imagery, preprocessing, feature extraction of spectral bands and vegetation indices, and RF classification to generate an operational per-pixel AGC surface. The model achieved $R^2 = 0.65$ with RMSE = 0.042 tons C/pixel (~1.05 tons C/ha), producing an operational per-pixel AGC surface. Mapped mangroves averaged 25.3 tons C/ha for a total of ~2,036.5 tons C. The overall map quality is supported by a robust mangrove mask (OA = 0.946; κ = 0.810). SWIR (B11–B12) was negatively associated with AGC, and TRVI showed a positive association, which helps mitigate NDVI/EVI saturation under dense canopies. Together, these features underpin the best predictions.

The novelty and contribution of this study lie in identifying SWIR and TRVI as the most informative predictors of AGC in small, fragmented mangroves and in demonstrating per-pixel scaling from field plots using open data and simple features. The small sample size (n = 15 plots) with limited spacing constrains ecological representativeness, so the AGC values should be interpreted cautiously. In practice, low-carbon zones should be prioritized for restoration, with *Avicennia marina* as a key pioneer species to accelerate recovery and enhance blue-carbon sequestration.

DATA AVAILABILITY

The dataset is available from the corresponding author upon reasonable request.

REFERENCES

[1] M. N. Sharabian, S. Ahmad, and M. Karakouzian, "Climate Change and Eutrophication: A Short Review," *Engineering, Technology & Applied Science Research*, vol. 8, no. 6, pp. 3668–3672, Dec. 2018, https://doi.org/10.48084/etasr.2392.

[2] R. Zhang and J. Fan, "Classification and Carbon-Stock Estimation of Mangroves in Dongzhaigang Based on Multi-Source Remote Sensing Data Using Google Earth Engine," *Remote Sensing*, vol. 17, no. 6, Mar. 2025, Art. no. 964, https://doi.org/10.3390/rs17060964.

[3] A. A. Md. A. P. Suardana *et al.*, "Estimation and Mapping Above-Ground Mangrove Carbon Stock Using Sentinel-2 Data Derived Vegetation Indices in Benoa Bay of Bali Province, Indonesia," *Forest and Society*, vol. 7, no. 1, pp. 116–134, Mar. 2023, https://doi.org/10.24259/fs.v7i1.22062.

[4] B. Choudhary, V. Dhar, and A. S. Pawase, "Blue carbon and the role of mangroves in carbon sequestration: Its mechanisms, estimation, human impacts and conservation strategies for economic incentives," *Journal of Sea Research*, vol. 199, Jun. 2024, Art. no. 102504, https://doi.org/10.1016/j.seares.2024.102504.

[5] A. Isdianto, A. W. Hasyim, B. M. Sukojo, I. Alimuddin, I. A. Anggraini, and E. R. Fatahillah, "Integrating Urban Design with Natural Dynamics: Enhancing Ecological Resilience in Malang City over a Decade," *International Journal of Sustainable Development and Planning*, vol. 20, no. 3, pp. 1061–1075, Mar. 2025, https://doi.org/10.18280/ijsdp.200313.

[6] B. S. Jasim, Z. T. Mohammed, and L. M. J. Mahdi, "Reliability of Data obtained by ASTER Satellite for Digital Elevation Models," *Engineering, Technology & Applied Science Research*, vol. 14, no. 5, pp. 17388–17392, Oct. 2024, https://doi.org/10.48084/etasr.8359.

[7] I. W. G. A. Karang, I. W. Nuarsa, I. G. Hendrawan, N. M. N. B. S. Dewi, P. K. Yasa, and I. M. D. Krisnanda, "Satellite remote sensing techniques for mapping and estimating mangrove carbon stocks in the small island of Gili Meno, West Nusa Tenggara, Indonesia," *Biodiversitas Journal of Biological Diversity*, vol. 25, no. 9, Oct. 2024, https://doi.org/10.13057/biodiv/d250941.

[8] H. J. Jumaah, N. K. Khursheed, V. F. Salahalden, and M. H. Ahmed Sulyman, "Integration of Remote Sensing and Artificial Intelligence in Detecting the Environmental Changes of Najaf Sea in Iraq Using NDWI and GIS," *Engineering, Technology & Applied Science Research*, vol. 15, no. 4, pp. 26107–26112, Aug. 2025, https://doi.org/10.48084/etasr.12265.

[9] N. Hidayah, "Studi penurunan luasan lahan mangrove di Kecamatan Ujungpangkah, Kabupaten Gresik," *Swara Bhumi*, vol. 5, no. 6, pp. 162–169, 2018.

[10] M. A. Asadi *et al.*, "Assessment of mangrove structures and biomass on islands along the Java Sea: a case study on Bawean Islands and Karimunjawa Islands," *Frontiers in Ecology and Evolution*, vol. 12, Sep. 2024, Art. no. 1422749, https://doi.org/10.3389/fevo.2024.1422749.

[11] M. Ali, Sulistiono, Z. Imran, and C. P. Simanjuntak, "The potential development of ecotourism based on mangrove ecosystem in Ujung Pangkah of Gresik Regency, East Java Province, Indonesia," *IOP Conference Series: Earth and Environmental Science*, vol. 800, no. 1, Jul. 2021, Art. no. 012054, https://doi.org/10.1088/1755-1315/800/1/012054.

[12] D. K. Saputra *et al.*, "Characteristics of Mangrove Fisheries in Essential Ecosystem Area Ujungpangkah, Indonesia," *Journal of Environmental Management and Tourism*, vol. 13, no. 3, Jun. 2022, Art. no. 812, https://doi.org/10.14505/jemt.v13.3(59).20.

[13] *Coastal Blue Carbon: Methods for Assessing Carbon Stocks and Emissions Factors in Mangroves, Tidal Salt Marshes, and Seagrass Meadows*. The Blue Carbon Initiative, 2014.

[14] E. Indrayani, J. Kalor, M. Warpur, and B. Hamuna, "Using Allometric Equations to Estimate Mangrove Biomass and Carbon Stock in Demta Bay, Papua Province, Indonesia," *Journal of Ecological Engineering*, vol. 22, no. 5, pp. 263–271, May 2021, https://doi.org/10.12911/22998993/135945.

[15] W. N. Aye, X. Tong, J. Li, and A. W. Tun, "Assessing the Carbon Storage Potential of a Young Mangrove Plantation in Myanmar," *Forests*, vol. 14, no. 4, Apr. 2023, Art. no. 824, https://doi.org/10.3390/f14040824.

[16] A. Komiyama, J. E. Ong, and S. Poungparn, "Allometry, biomass, and productivity of mangrove forests: A review," *Aquatic Botany*, vol. 89, no. 2, pp. 128–137, Aug. 2008, https://doi.org/10.1016/j.aquabot.2007.12.006.

[17] F. Sidik, D. W. Kusuma, H. P. Kadarisman, and Suhardjono, *Panduan Mangrove: Survei Ekologi dan Pemetaan*. 2019.

[18] F. Sidik, N. Widagti, and H. P. Kadarisman, *Mangrove dan Perubahan Iklim: Panduan Stasiun Monitoring Mangrove*. 2019

[19] M. Muhamad, D. H. Santosa, E. N. Kardiyati, and M. A. R. Putra, "Mapping Above-Ground Mangrove Ecosystems for Nature Tourism Routes to Support Sustainable Tourism Development in South Lembar Village, West Nusa Tenggara," *Jurnal Pengabdian kepada Masyarakat (Indonesian Journal of Community Engagement)*, vol. 11, no. 2, Jun. 2025, Art. no. 72, https://doi.org/10.22146/jpkm.100828.

[20] Y. Zhu *et al.*, "Exploring the Potential of WorldView-2 Red-Edge Band-Based Vegetation Indices for Estimation of Mangrove Leaf Area Index with Machine Learning Algorithms," *Remote Sensing*, vol. 9, no. 10, Oct. 2017, Art. no. 1060, https://doi.org/10.3390/rs9101060.

[21] M. Qasim and E. Csaplovics, "AGB estimation using Sentinel-2 and Sentinel-1 datasets," *Environmental Monitoring and Assessment*, vol. 196, no. 3, Mar. 2024, Art. no. 299, https://doi.org/10.1007/s10661-024-12478-5.

[22] E. Purnamasari, M. Kamal, P. Wicaksono, M. F. Hidayatullah, and B. B. Susetyo, "Multi-spatial Resolution Imagery to Estimate Above-Ground Carbon Stocks in Mangrove Forests," *JOIV : International Journal on Informatics Visualization*, vol. 8, no. 3, Sep. 2024, Art. no. 1118, https://doi.org/10.62527/joiv.8.3.2237.

[23] S. S. Rijal, T. D. Pham, S. Noer'Aulia, M. I. Putera, and N. Saintilan, "Mapping Mangrove Above-Ground Carbon Using Multi-Source Remote Sensing Data and Machine Learning Approach in Loh Buaya, Komodo National Park, Indonesia," *Forests*, vol. 14, no. 1, Jan. 2023, Art. no. 94, https://doi.org/10.3390/f14010094.

[24] Z. Shen, J. Miao, J. Wang, D. Zhao, A. Tang, and J. Zhen, "Evaluating Feature Selection Methods and Machine Learning Algorithms for Mapping Mangrove Forests Using Optical and Synthetic Aperture Radar Data," *Remote Sensing*, vol. 15, no. 23, Dec. 2023, Art. no. 5621, https://doi.org/10.3390/rs15235621.

[25] S. Manna and B. Raychaudhuri, "Mapping distribution of Sundarban mangroves using Sentinel-2 data and new spectral metric for detecting their health condition," *Geocarto International*, vol. 35, no. 4, pp. 434–452, Mar. 2020, https://doi.org/10.1080/10106049.2018.1520923.

[26] M. Natarajan, S. Ayyappan, and M. Vajiravelu, "Carbon stock assessment on natural mangrove species of Avicennia marina in Pichavaram mangrove forest Southeast coast of India." In Review, Sep. 06, 2022, https://doi.org/10.21203/rs.3.rs-1274783/v1.

[27] R. Shawky, "Carbon Sink potentiality of Avicennia marina along the Egyptian Red Sea Coast." In Review, Nov. 23, 2023, https://doi.org/10.21203/rs.3.rs-3634079/v1.

[28] A. L. Fathah, B. Semedi, F. C. Wardana, and A. Isdianto, "Assessment of Mangrove Diversity, Biomass, and Carbon Stocks in the Ujungpangkah Estuary, Gresik," *Journal of Environmental Engineering and Sustainable Technology*, vol. 12, no. 1, pp. 25–34, Aug. 2025.

[29] R. Rudianto, D. G. Bengen, and F. Kurniawan, "Causes and Effects of Mangrove Ecosystem Damage on Carbon Stocks and Absorption in East Java, Indonesia," *Sustainability*, vol. 12, no. 24, Dec. 2020, Art. no. 10319, https://doi.org/10.3390/su122410319.

[30] V. B. Arifanti, J. B. Kauffman, Subarno, M. Ilman, A. Tosiani, and N. Novita, "Contributions of mangrove conservation and restoration to climate change mitigation in Indonesia," *Global Change Biology*, vol. 28, no. 15, pp. 4523–4538, Aug. 2022, https://doi.org/10.1111/gcb.16216.